Since January 2020 Elsevier has created a COVID-19 resource centre with free information in English and Mandarin on the novel coronavirus COVID-19. The COVID-19 resource centre is hosted on Elsevier Connect, the company's public news and information website.

Journal of Structural Biology 177 (2012) 168–176

Contents lists available at SciVerse ScienceDirect

Journal of Structural Biology

journal homepage: www.elsevier.com/locate/yjsbi

Optimizing the refolding conditions of self-assembling polypeptide nanoparticles that serve as repetitive antigen display systems

Yongkun Yang [a], Philippe Ringler [b,1], Shirley A. Müller [b,1], Peter Burkhard [a,c,*]

[a] Institute of Materials Science, University of Connecticut, 97 N. Eagleville Road, Storrs, CT 06269, USA
[b] Maurice E. Müller Institute for High Resolution Electron Microscopy, Biozentrum, University of Basel, Klingelbergstrasse 50/70, CH 4054 Basel, Switzerland
[c] Department of Molecular and Cell Biology, University of Connecticut, 91 N. Eagleville Road, Storrs, CT 06269, USA

ARTICLE INFO

Article history:
Available online 17 November 2011

Keywords:
Self-assembly
Peptide nanoparticles
Coiled coils
Protein folding
Mass measurement
Scanning transmission electron microscopy

ABSTRACT

Nanoparticles show great promise as potent vaccine candidates since they are readily taken up by the antigen presenting cells of the immune system. The particle size and the density of the B cell epitopes on the surface of the particles greatly influences the strength of the humoral immune response. We have developed a novel type of nanoparticle composed of peptide building blocks (Raman et al., 2006) and have used such particles to design vaccines against malaria and SARS (Kaba et al., 2009; Pimentel et al., 2009). Here we investigate the biophysical properties and the refolding conditions of a prototype of these self-assembling polypeptide nanoparticles (SAPNs). SAPNs are formed from a peptide containing a pentameric and a trimeric coiled-coil domain. At near physiological conditions the peptide self-assembles into about 27 nm, roughly spherical SAPNs. The average size of the SAPNs increases with the salt concentration. The optimal pH for their formation is between 7.5 and 8.5, while aggregation occurs at lower and higher values. A glycerol concentration of about 5% v/v is required for the formation of SAPNs with regular spherical shapes. These studies will help to optimize the immunological properties of SAPNs.

1. Introduction

Self-assembly is the process by which components are spontaneously organized into ordered structures without external intervention (Whitesides and Grzybowski, 2002). Self-assembly phenomena are ubiquitous in nature, especially in biological systems including peptides, proteins, nucleic acids, and lipids (Whitesides and Grzybowski, 2002; Zhang, 2003). Inspired by nature, molecular self-assembly processes are intensively exploited to create novel nanoscale biomaterials. Drexler (1981) first proposed that engineered proteins could be used as monomeric building blocks to fabricate devices through self-assembly approaches. Since then peptides and proteins have become abundant and versatile building blocks (Gazit, 2007; Rajagopal and Schneider, 2004; Subramani et al., 2008; Toksöz and Guler, 2009; Tsai et al., 2007; Yang et al., 2009; Zhang, 2002; Zhang et al., 2002). They are now used to engineer nanorings (Carlson et al., 2006), nanotubes (Scanlon and Aggeli, 2008), nanofibrils (Yang et al., 2009; Zhang, 2002, 2003; Zhang et al., 2002), nanoparticles (Kaba et al., 2009; Raman et al., 2006, 2009) and other ordered structures at the nanoscale (Carlson et al., 2006). They can also form mesoscopic and macroscopic structures with nanoscale order (Whitesides and Boncheva, 2002), such as monolayers (Rapaport et al., 2000), hydrogels (Petka et al., 1998) and three-dimensional scaffolds (Holmes, 2002; Zhang et al., 2005). Peptides and proteins possess many advantages, such as biocompatibility, chemical diversity and bioactivity. Thus, self-assembling peptides and proteins have enormous potential applications in the field of nanobiotechnology.

The self-assembly of peptides is controlled by their amino acid sequence and secondary structure. Peptide self-assembly is mainly governed by the non-covalent interactions among the main and side chain atoms. The non-covalent interactions stabilize the nanostructures of the self-assembled peptides through the formation of secondary structures such as β-sheets and α-helices (Fairman and Åkerfeldt, 2005; Rajagopal and Schneider, 2004; Toksöz and Guler, 2009; Zanuy et al., 2006).

α-Helical coiled coils are the most common oligomerization motif found in proteins (Burkhard et al., 2001) and are capable of forming extremely stable and well defined oligomers. Some well-known examples are the coiled-coil domains of the GCN4 leucine zipper (O'Shea et al., 1991), fibritin (Tao et al., 1997), tetrabrachion

Abbreviations: CD, circular dichroism; DLS, dynamic light scattering; LB, Luria Broth; MW, molecular weight; SAPN, self-assembling polypeptide nanoparticle; SDS–PAGE, sodium dodecyl sulfate–polyacrylamide gel electrophoresis; SE, standard error; STEM, scanning transmission electron microscopy/microscope; TEM, transmission electron microscopy/microscope; TMV, tobacco mosaic virus.

* Corresponding author at: Institute of Materials Science, University of Connecticut, 97 N. Eagleville Road, Storrs, CT 06269, USA. Fax: +1 860 486 4745.
E-mail address: peter.burkhard@uconn.edu (P. Burkhard).
[1] Present address: Center for Cellular Imaging and Nano Analytics (C-CINA), Biozentrum, University of Basel, Mattenstrasse 26, CH-4058 Basel, Switzerland.

1047-8477/$ - see front matter © 2011 Elsevier Inc. All rights reserved.
doi:10.1016/j.jsb.2011.11.011

(Stetefeld et al., 2000), and the cartilage oligomerization matrix protein (COMP) (Malashkevich et al., 1996), which represent dimeric, trimeric, tetrameric, and pentameric coiled coils, respectively. α-Helical coiled coils are convenient building blocks for the design of self-assembling nanostructures. We have designed a novel type of self-assembling polypeptide nanoparticle (SAPN) with well-defined size and shape using the slightly modified pentameric coiled-coil domain of COMP and a *de novo*-designed trimeric coiled-coil domain in which the two oligomerization domains are joined by a two-glycine residue linker (Raman et al., 2006). The design was based on an icosahedral model (Padilla et al., 2001; Raman et al., 2006) in which the two rotational symmetry axes from the pentameric and trimeric coiled-coil domains are superpositioned onto the fivefold and threefold symmetry axes of the icosahedron. Upon formation of the coiled coils from the two oligomerization domains, the peptides self-assemble into nanoparticles. Ideally the SAPN would have icosahedral symmetry and accommodate 60 peptide chains per particle in a $T = 1$ icosahedron (Fig. 1D, top), or 180 chains in a $T = 3$-like icosahedron (Fig. 1D, bottom).

We have successfully used such SAPNs with regular symmetry as a repetitive antigen display system (Kaba et al., 2009; Pimentel et al., 2009; Schroeder et al., 2009). Peptide epitopes can easily be engineered at either end of the peptide sequence of the SAPN, which results in the repetitive display of epitopes, which in turn is able to generate a strong immune response (Fehr et al., 1998). For example such SAPNs have been used as a platform to present the tandem repeat of the B cell immunodominant repeat epitope $(DPPPPNPN)_2D$ of the circumsporozoite protein of the malaria parasite *Plasmodium berghei* (Kaba et al., 2009), the HRC1 epitope of the spike protein from the severe acute respiratory syndrome coronavirus (Pimentel et al., 2009), and the hydrophobic loop of actin (Schroeder et al., 2009). All of these studies have demonstrated that specific immune responses towards the projected epitopes were elicited by the repetitive display of the epitopes on the surface of the SAPNs, indicating the potential of the SAPN as an antigen display system in the design of novel vaccines.

To develop SAPNs into a valuable platform for vaccine design, we have now analyzed their biophysical properties in more detail using circular dichroism (CD) spectroscopy, negative stain transmission electron microscopy (TEM), digital light scattering (DLS), and scanning transmission electron microscopy (STEM). Factors that influence the formation and stability of coiled coils, including pH, temperature, ionic strength and glycerol concentration were investigated to define the best refolding conditions for SAPN formation. These studies will help to optimize the size of the nanoparticles and the density of the B cell epitope on the surface of the SAPN, factors that are critically important for the generation of a strong immune response as shown decades ago (Aebi et al., 1977; Dintzis et al., 1976).

2. Materials and methods

2.1. Expression and purification of P6c peptide

The modified pPEP-T vector (Kammerer et al., 1998) containing the code for the P6c peptide was transformed into the *Escherichia coli* strain BL21(DE3)pLysS expression cells (Novagen, Madison, WI, USA). The bacteria were incubated at 37 °C in Luria Broth (LB) medium in the presence of 200 mg/ml ampicillin and 30 mg/ml chloramphenicol. Expression was induced by adding 1 mM isopropyl β-D-thiogalactopyranoside. After 3 h of expression, the bacteria were collected by centrifugation at 4000*g* for 15 min. The bacterial pellet was resuspended and lysed in a lysis buffer (9 M urea, 100 mM NaH_2PO_4, 10 mM Tris, 10 mM β-mercaptoethanol, pH 8.0) by sonication. The cell debris was removed by centrifugation at 30,500 *g* for 45 min. The supernatant was incubated with Ni-NTA Agarose beads (Qiagen, Valencia, CA, USA) overnight and then loaded into a column. The protein contaminants were removed by washing the column sequentially with buffers containing 9 M urea, 100 mM NaH_2PO_4, 20 mM sodium citrate, 10 mM imidazole and 10 mM β-mercaptoethanol at pH 6.3, 5.9 and 5.0. The P6c peptides were then eluted using elution buffer containing 9 M urea, 100 mM NaH_2PO_4, 10 mM Tris, 500 mM imidazole, 10 mM β-mercaptoethanol pH 8.0. The purity of the P6c peptides was verified by SDS–PAGE.

2.2. SAPN preparation

The typical refolding procedure for the P6c peptide was as follows: The P6c peptide was denatured in a urea-containing buffer (9 M urea, 20 mM HEPES pH 7.5, 150 mM NaCl, 5% glycerol), and concentrated to 1 mg/ml. The peptide was then refolded by rapid dilution (ratio of 20:1) by adding it dropwise to a larger volume of refolding buffer (e.g., 20 mM HEPES pH 7.5, 150 mM NaCl, 5% glycerol), until a peptide concentration of 0.05 mg/ml had been reached. The samples were then dialyzed overnight in the refolding buffer to remove the remaining urea.

The effect of salt on the SAPNs was tested in refolding buffers containing 20 mM HEPES at pH 7.5, 5% glycerol and seven different NaCl concentrations (0, 50, 100, 150, 200, 300, and 500 mM, respectively).

The effect of pH on the SAPNs was tested in five refolding buffers: pH 7.0 (20 mM BES), pH 7.5 (20 mM HEPES), pH 8.0 (20 mM Tris), pH 8.5 (20 mM Bicine), and pH 9.0 (20 mM CHES), respectively. All the buffers contained 150 mM NaCl and 5% glycerol.

The effect of glycerol on the SAPNs was tested in refolding buffers containing 20 mM HEPES pH 7.5, 150 mM NaCl, and five different concentrations of glycerol (0%, 2.5%, 5%, 10% and 15% v/v, respectively).

2.3. Circular dichroism (CD) spectroscopy

CD experiments were performed in an Applied Photophysics Pi Star 180 spectrapolarimeter at 20 °C. CD spectra were recorded from 190 to 250 nm in 20 mM sodium phosphate pH 7.5, 150 mM NaCl, 5% glycerol. Temperature denaturation profiles were obtained with a 1 mm path length cell at 0.65 mg/ml protein concentration by following the change in molar ellipticity at 222 nm from 6 to 90 °C and a temperature increase rate of 1 °C/min.

2.4. Dynamic Light Scattering (DLS)

The hydrodynamic diameter was determined with a Malvern Zetasizer Nano S equipped with a 633 nm laser. The measurements were made at 20 °C unless otherwise indicated.

The effect of temperature on the SAPNs was tested in 20 mM sodium phosphate pH 7.5, 150 mM NaCl, 5% glycerol. The samples were heated to the desired temperature and equilibrated for 3 min. Measurements were performed at 20, 37, 45, 65, and 85 °C.

2.5. Transmission Electron Microscopy (TEM)

Samples were adsorbed for formvar/carbon coated grids (Electron Microscopy Sciences Inc., Hatfield, PA, USA) that had been subjected to a 15 s glow discharge in a low pressure of air, washed with distilled water twice, and negatively stained with 1% uranyl acetate (Structure Probe Inc., West Chester, PA, USA). Electron micrographs were taken on an FEI Tecnai T12 TEM at an accelerating voltage of 80 kV.

The TEM images were first inspected with Photoshop CS4 (Adobe, San Jose, CA). The particles were selected and filled manually using

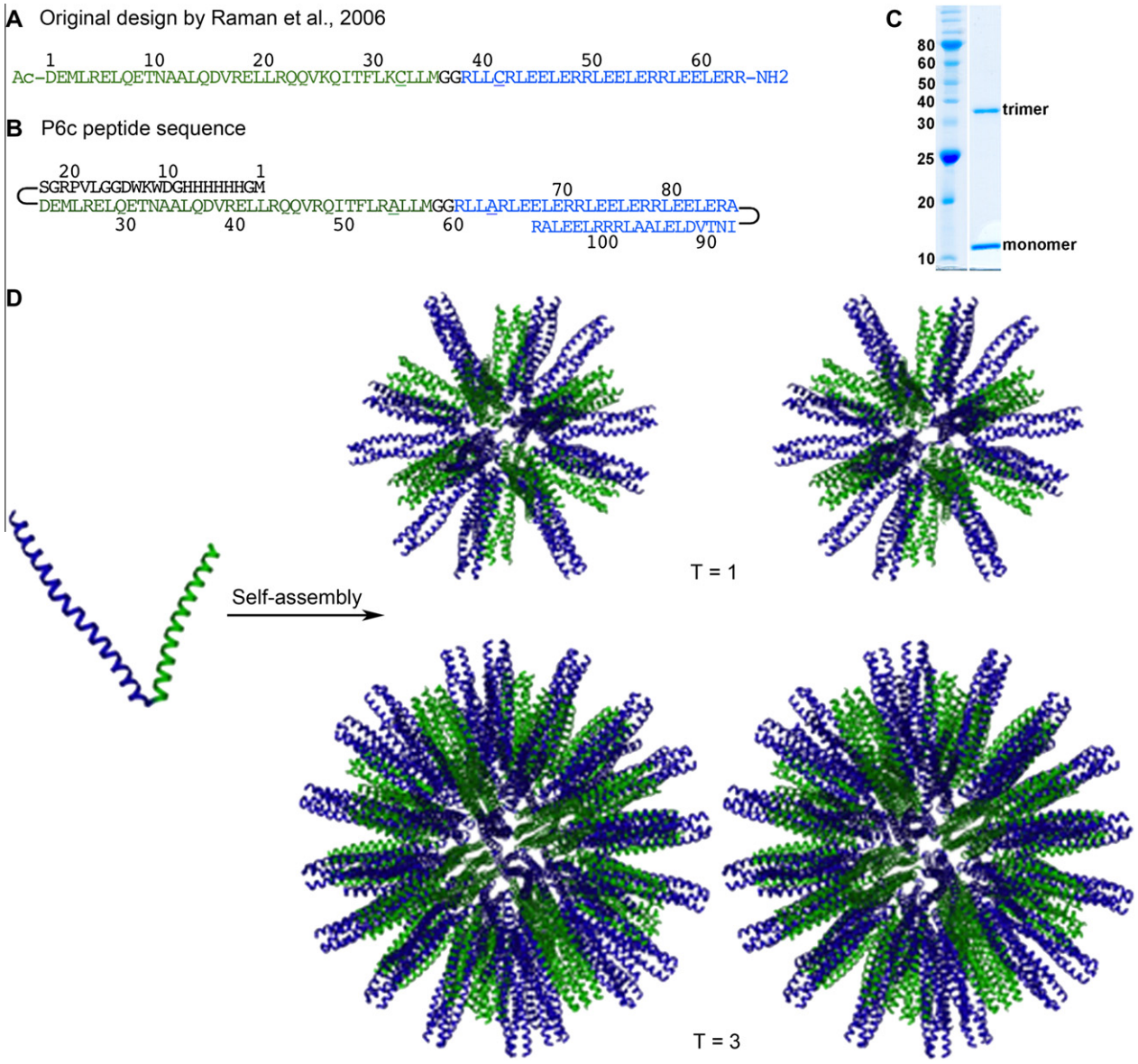

Fig.1. (A) Sequence of the 7.9 kDa peptide construct originally designed by Raman et al. (2006) and (B) of the 12.6 kDa P6c peptide. In both cases the two-glycine residue linker is in black type. (C) Coomassie blue stained SDS–PAGE gel of the P6c peptide sample. Left: relative molecular weight markers (kDa) Right: P6c peptide. (D) Left: 3D representation of the P6c peptide. Blue; trimeric coiled coil domain. Green; pentameric coiled coil domain. The his-tag is not shown. When multiple coiled coils form from the two oligomerization domains the peptides self-assemble into a SAPN. Right: Stereo picture of computer models of the P6c SAPN with $T = 1$ (top, 60 peptides) and $T = 3$ (bottom, 180 peptides) icosahedral symmetry with calculated diameters of about 20 and 25 nm, respectively. The his-tag is not shown.

the selection tools in Photoshop CS4, omitting the very small particles or background (area less than 50 nm^2) and large aggregates (area larger than 5000 nm^2). Image analysis was then performed with the public domain software ImageJ (Rasband, 1997). Then, the Feret diameters obtained by ImageJ were used to describe the sizes of the particles.

2.6. Scanning transmission electron microscopy (STEM)

The nanoparticles were at a concentration of 0.1 mg/ml in 20 mM HEPES pH 7.5, 150 mM NaCl, 5% glycerol. Glycerol was removed from the undiluted sample using spin columns following the Zeba™ Desalt Spin Column Instructions (Pierce). The nanoparticles were subsequently diluted 8× in buffer without glycerol and a 5 µl aliquot was immediately adsorbed for 1 min to a glow discharged STEM film (thin carbon film that spans a thick fenestrated carbon layer covering 200-mesh/inch, gold-plated copper grids). The grid was then blotted, washed on eight drops of quartz double-distilled water, blotting between each step, and plunge frozen in liquid nitrogen. It was freeze-dried at −80 °C and 5×10^{-8} Torr overnight in the microscope. Tobacco mosaic virus (TMV) particles (kindly provided by R. Diaz Avalos) served as a mass standard. These particles were similarly adsorbed to separate STEM films, washed on eight drops of 100 mM ammonium bicarbonate and air-dried.

A Vacuum Generators HB-5 STEM interfaced to a modular computer system (Tietz Video and Image Processing System GmbH, Gauting, Germany) was employed. Series of 512 × 512-pixel, dark-field images were recorded from the unstained sample at an acceleration voltage of 80 kV and a nominal magnification of 200,000×. The recording dose was 344 ± 11 electrons/nm^2. Regions of the freeze-dried sample were also repeatedly scanned to determine the beam-induced mass-loss. The digital images were evaluated using the program package MASDET (Krzyžánek et al., 2009).

In short, projections were selected in circular boxes, the total scattering of each region calculated, the average background scattering of the carbon support film subtracted and the mass calculated. The results were scaled according to the mass-per-length measured for TMV, corrected for beam-induced mass-loss (Müller et al., 1992), binned into histograms and described by a series of Gauss curves. The overall experimental uncertainty was estimated from the corresponding standard error (SE = SD/$\sqrt{}$n) and the ~5% uncertainty in the calibration of the instrument. Nanoparticles with masses in operator-defined ranges centered at the peak maxima were sorted into galleries for inspection.

2.7. Model building

The model for the $T = 1$ icosahedron was built as described in (Raman et al., 2006), putting one peptide chain in the asymmetric unit of the icosahedron between the pentameric and the trimeric rotational axes. For the $T = 3$ icosahedron, three peptide chains were placed into one asymmetric unit according to the requirements for $T = 3$ icosahedral symmetry in which the three chains of the asymmetric unit are only quasi-equivalent. This requires smaller angles between the pentamer and the trimer domain and a larger distance of the chains from the center of the icosahedron, thus leading to a diameter of the nanoparticles of about 25 nm instead of the 20 nm for the $T = 1$ icosahedral model.

3. Results

The sequence of the peptide we originally designed and chemically synthesized for nanoparticle formation (Raman et al., 2006) is shown in Fig. 1A. The related peptide of this study, "P6c", contains an additional His-tag sequence (22 amino acids) at the N-terminus and a longer trimeric coiled-coil domain at the C-terminus (20 amino acids; Fig. 1B). Furthermore, the two cysteine residues in the original design were replaced by alanine residues (A55 and A64 in P6c) in an attempt to avoid aggregation caused by the formation of intermolecular disulfide bridges. The His-tag facilitates the purification process after recombinant protein expression in *E. coli*. The trimeric domain was extended by three heptad repeats to increase the stability of the trimeric coiled coil (Burkhard et al., 2000a,b, 2002,). The engineered P6c peptide has a calculated molecular weight of 12.6 kDa. On SDS–PAGE it ran as two bands one at a relative molecular weight (MW) of about 12 kDa corresponding to a monomer, and the other at the relative MW of about 36 kDa corresponding to a trimer (Fig. 1C). The presence of trimers on the denaturing SDS–PAGE gels implies that the P6c peptide indeed forms a very stable trimeric coiled coil. Modeling predicts that when trimeric and pentameric coiled coils form from the two P6c oligomerization domains the SAPN will either accommodate 60 peptides in $T = 1$ icosahedral symmetry and have a diameter of about 20 nm or accommodate 180 peptide chains in $T = 3$-like icosahedral symmetry and have a diameter of about 25 nm (Fig. 1D).

3.1. Biophysical properties of SAPNs at close to physiological conditions

The secondary structure of the P6c peptide in 20 mM sodium phosphate pH 7.5, 150 mM NaCl, 5% glycerol was examined by CD spectroscopy. For optical reasons the otherwise used HEPES buffer was replaced with phosphate buffer. The spectra have double minima at 208 and 222 nm, which are characteristic of α-helical structures (Fig. 2A). The temperature denaturation profile shows that only ~10% of the peptide was unfolded at 90 °C, again indicating that the α-helices in the P6c peptide are extremely thermostable (Fig. 2B). Hence the nanoparticles are expected to be stable, even at very high temperature.

TEM revealed that under the close to physiological conditions of 20 mM HEPES pH 7.5, 150 mM NaCl, 5% glycerol P6c peptides self-assemble into SAPNs with roughly circular projections (Fig. 3A) 20–35 nm in diameter, the average diameter being about 27 nm (Fig. 3B). The size distribution of the SAPNs was also analyzed by DLS, which gave a volume-average hydrodynamic diameter of 28 nm with a standard deviation of about 10 nm (Fig. 3B).

Circular projections are compatible with a spherical shape, but could also be top views of a cylindrical structure, and indeed various elongated structures were sometimes observed on the TEM images. To obtain further information, quantitative dark-field scanning transmission electron microscopy (STEM) was employed to measure the molecular masses of the SAPNs. This single molecule technique determines the mass of individual particles from images of unstained samples by integrating the electron scattering with appropriate background subtraction (see Section 2). Further, the images allow mass to be directly linked to particle shape. The mass of over 300 P6c SAPNs was determined (Fig. 4A). The resulting histogram indicates the presence of one major and several minor particle populations. Accordingly, most of the SAPNs (63.5%) have a mass of 2.23 (±0.46) MDa (SE, ±0.03 MDa; overall uncertainty, ±0.12 MDa), and with few exceptions, almost circular projections (Fig. 4B). The smaller particle populations have masses of 3.76, 4.41 and 6.76 (±0.46) MDa, respectively and their projections are larger, generally elongated and sometimes clearly arise from particle association. The results indicate that most SAPNs are indeed almost spherical in shape. Deviations might be due to the presence of the N-terminal sequence of 22 amino acids

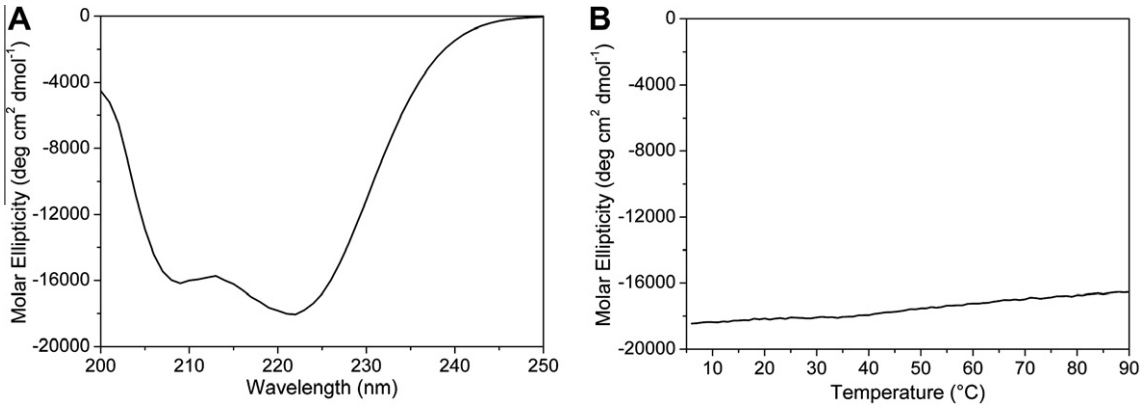

Fig.2. Physical properties of SAPNs (A) Far-UV CD spectrum of the P6c peptide in 20 mM sodium phosphate pH 7.5, 150 mM NaCl, 5% glycerol. The peptide concentration was 0.4 mg/ml. (B) Temperature denaturation profile of the P6c peptide. The profile was monitored by CD at a wavelength of 222 nm.

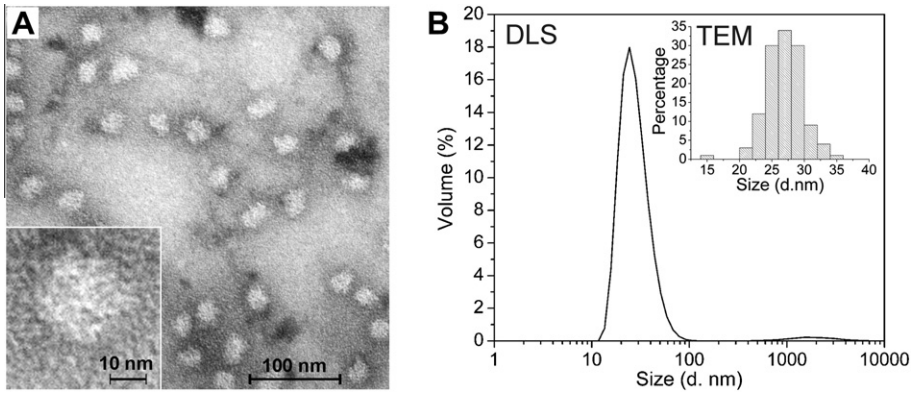

Fig.3. SAPN morphology and dimensions (A) TEM image of P6c SAPNs. The sample was negatively stained with 1% uranyl acetate. The peptide concentration was 0.05 mg/ml and the buffer was 20 mM HEPES pH 7.5, 150 mM NaCl, 5% glycerol. An enlarged view of one SAPN is shown in the inset. (B) Size distribution of the SAPNs. The volume distribution profile from the dynamic light scattering measurement shows a peak corresponding to a hydrodynamic diameter of 28 nm. The TEM microscopy indicated an average diameter of 27 nm (n = 190).

containing the His-tag. This sequence does not form a coiled coil but rather is a flexible peptide at the surface of the SAPN. SAPNs with a particle mass of 2.23 MDa must be formed by approximately 180 peptide chains (177 ± 10 considering the overall uncertainty), which would correspond to a $T = 3$ icosahedron-like structure. The small population with a particle mass of 3.76 MDa (SE, ±0.07 MDa; overall uncertainty, ±0.20 MDa) indicated by the second histogram peak must comprise approximately 300 peptide chains, which is in accordance with their somewhat elongated structure; this might be a unique structure or, as evident for some of the projections, arise from the association of two lower mass SAPNs. The SAPNs in the third and fourth peaks have more irregular shapes and appear to be aggregated particles of roughly the same size as those giving rise to peak 1.

3.2. The effects of refolding conditions on SAPNs

3.2.1. Salt concentration

Various refolding conditions were used to examine and optimize the refolding and resulting SAPN formation. The influence of additional salt at various concentrations on the self-assembly process of the P6c peptide was examined first, using buffers containing 20 mM HEPES pH 7.5 and 5% glycerol and various NaCl concentrations. The SAPNs formed were quite homogeneous and, as judged from their almost circular projections on TEM images, spherical in buffers with NaCl concentrations up to 300 mM (Fig. 5A–F). At 500 mM NaCl the SAPNs were less homogeneous and were prone to aggregate (Fig. 5G). Overall, the average size of the SAPNs determined by DLS and TEM increased with increasing salt concentration. The average hydrodynamic size of the SAPNs formed changed from 20 nm (width 7.5 nm) to 35 nm (width 17.7 nm), when the NaCl concentration increased from 0 to 500 mM (Fig. 5H). This was corroborated by the particle dimensions measured by TEM; the average particle diameter increased from 19 ± 3 nm (n = 145) at 0 mM NaCl to 31 ± 7 nm (n = 69) at 500 mM NaCl (Fig. 5I). The size distribution of the SAPNs was much broader at 500 mM NaCl, which might be partially attributed to increasing levels of aggregation.

3.2.2. pH

The effect of pH on SAPN formation was tested at constant salt (150 mM NaCl) and glycerol (5%) concentration. The P6c peptide was refolded in five different buffers ranging from pH 7.0 to pH 9.0 (see Section 2). As judged from the almost circular projections on TEM images, the peptide self-assembled into the nicest spherical SAPNs at pH 7.5–8.0 (Fig. 6B–C). Aggregation occurred at pH 7.0 (Fig. 6A). At pH 8.5 (Fig. 6D) SAPN morphology changed slightly and there was a background of smaller particles possibly because self-assembly was not so efficient. There was again aggregation at pH 9.0 (Fig. 6E). As might be expected from these images, analysis by DLS showed that the SAPNs formed at pH 7.5, 8.0 and 8.5 had similar average hydrodynamic sizes of about 30 nm. The average hydrodynamic sizes were larger at pH 7.0 (80 nm) and at pH 9.0 (37 nm) (Fig. 6F, G). The size distribution of the SAPNs at pH 7.0 and 9.0 was broader than at pH 7.5–8.5 most likely due to the onset of aggregation. In agreement with the DLS data, the average SAPN diameters indicated by negative stain TEM were 26 ± 5 nm (n = 108) at pH 7.5 and 29 ± 5 nm (n = 211) at pH 8.0 and 31 ± 6 nm (n = 74) at pH 8.5 (Fig 6G).

3.2.3. Glycerol concentration

The influence of glycerol on the self-assembly of P6c to SAPNs was tested in 20 mM HEPES pH 7.5, 150 mM NaCl; 0%, 2.5%, 5%, 10%, or 15% v/v glycerol was added. Many of the SAPNs have elongated shapes at low glycerol concentrations of 0% and 2.5% and form rope-like structures (Fig. 7A and B). From the almost circular projections on TEM images, spherical and discrete SAPNs are formed at the intermediate glycerol concentrations of 5% and 10% (Fig. 7C and D), while at higher glycerol concentration (15%) the SAPNs have irregular shapes and start to aggregate (Fig. 7E). According to DLS experiments the smallest average hydrodynamic size of the SAPNs, 28 nm, was obtained at 5% glycerol (Fig. 7F and G). The size distribution of the SAPNs was also narrowest at 5% glycerol. In contrast, the SAPNs displayed a very broad size distribution at 15% glycerol, implying that higher glycerol concentration causes aggregation. The average SAPN diameters at 2.5%, 5% and 10% glycerol indicated by negative stain TEM were in good agreement wit the DLS data (Fig 6G).

3.2.4. Temperature

According to their CD spectra the SAPNs formed are thermally very stable (Fig. 2), This allowed DLS measurements to be carried out at several different temperatures between 20 and 85 °C. The effect of temperature on the size and size distribution of the SAPNs is summarized in Fig 8. As shown in Fig. 8A, the average hydrodynamic size of the SAPNs decreased from 30 to 23 nm as the temperature rose from 20 to 85 °C. The presence of the DLS peak of 23 nm at 85 °C implies that the SAPNs still exist at this high temperature, although TEM images of the samples are not available.

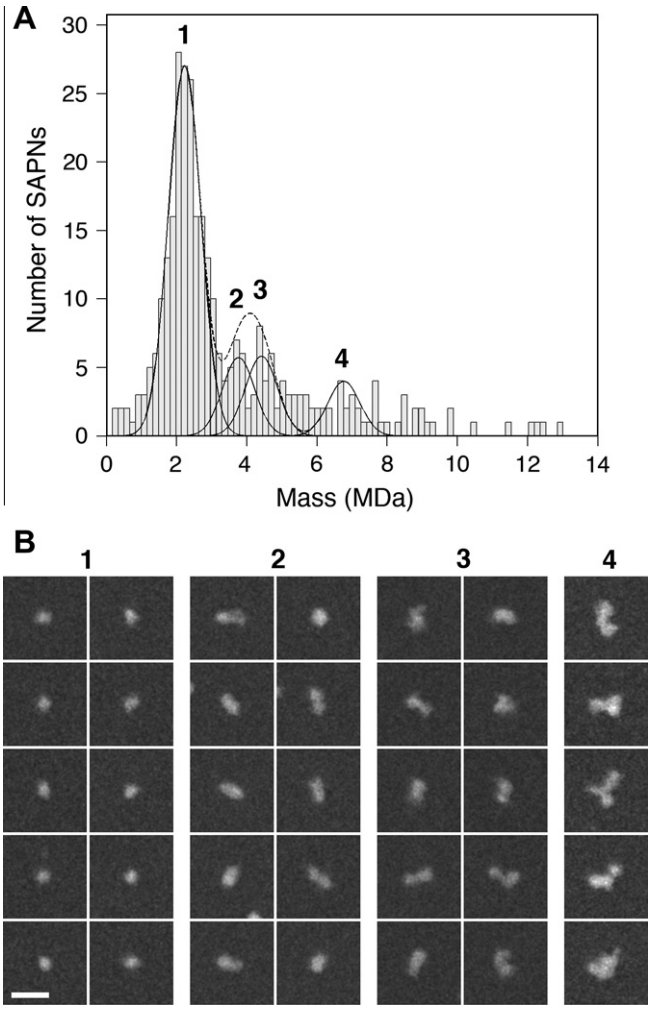

Fig.4. SAPN mass determined by STEM (A) Histogram showing the mass distribution of the SAPNs in 20 mM HEPES pH 7.5, 150 mM NaCl (without glycerol). Most of the data can be described by four Gaussian curves of equal width; the peak envelope is shown by the dotted line. The major peak is centered at 2.23 (±0.46) MDa (SE, ±0.03 MDa; overall uncertainty ±0.12 MDa) and the minor peaks at 3.76, 4.41 and 6.76 (±0.46) MDa, (SEs, ±0.07, ±0.7 and ±0.09 MDa; overall uncertainties, ±0.20, ±0.23 and ±0.35 MDa, respectively). (B) Galleries showing representative dark-field STEM images of the SAPNs within each peak. Scale bar represents 50 nm.

4. Discussion

Coiled-coil formation and stability is a prerequisite for the self-assembly of P6c peptides into nanoparticles and for the persistence of their epitope decorated counterparts after patient vaccination. The hydrophobic interactions along the coiled-coil interface are the main driving force for coiled-coil formation. Many other factors also contribute to their stability. For example, coiled coils can be stabilized by a complex network of inter- and intrahelical salt bridges (Burkhard et al., 2000a, 2002; Meier and Burkhard, 2006; Meier et al., 2010). Indeed, removing a single interhelical salt bridge can even abolish coiled-coil formation (Meier et al., 2002). The geometry between the pentameric and trimeric coiled coils formed on P6c oligomerization is important for SAPN formation (Fig. 1). This geometry is constrained by the conformation of the residues around the two-glycine residue linker (Fig 1B) and influenced by interactions with the neighboring coiled coils as SAPNs form, which can be hydrophobic, electrostatic, hydrogen bonding and Van der Waals in nature. All of these non-covalent interactions are affected by the buffer conditions employed such as salt concentration, pH, temperature, and co-solvents e.g., glycerol. Glycerol is a very commonly used co-solvent, and is thought to decrease the diffusivity and the partial molar volume of proteins inhibiting aggregation (Meng et al., 2001). The large increases in solvent viscosity it causes are accompanied by relatively small changes of the pH and dielectric constant (Schein, 1990).

The geometrical constraints operating on the two oligomerization domains of the P6c peptide, when trimers and pentamers form lead to the self-assembly of nanoparticles and define their shape (Raman et al., 2006; Zandi et al., 2004). If formed by P6c as predicted, SAPNs with the $T = 1$ icosahedral symmetry (Fig. 1D, top; Raman et al., 2006) would have a diameter of 20 nm and accommodate 60 peptides. In the original design, two cystein residues present (Fig. 1A) either formed intramolecular disulfide bonds giving the SAPNs a degree of angular rigidity (Raman et al., 2006; Zandi et al., 2004) or, as experiment showed, intermolecular disulfide bonds leading to aggregation (Raman et al., 2006). Replacement of these two residues by alanine in P6c significantly reduced particle aggregation under close to native conditions (compare Fig. 3A with Fig. 3A of Raman et al., 2006). However, some particle heterogeneity was still visible on TEM images. This may be due to residual aggregation and/or be because the P6c SAPNs do not always have strict icosahedral symmetry. The increased flexibility of the two-glycine residue linker in the P6c peptide chain in the absence of the disulfide bridge, could make the latter possible; in P6c the two coiled-coil domains are no longer restrained, their relative angular orientation can vary and, as a consequence, the SAPNs can incorporate different numbers of peptide chains per particle leading to different nanoparticle sizes. These two scenarios, simple nanoparticle aggregation (i.e., two, three or more particles sticking together) versus a size increase because the geometry and stoichiometry of the nanoparticles changes (i.e., elongated structures formed), will give very similar results in some biophysical analyzes, e.g., in DLS experiments. Thus, the DLS measurements made in the present work to obtain the overall average hydrodynamic radius of the nanoparticles present in the P6c under different conditions, were complemented by electron micrsoscopy. Negative stain TEM generally sufficed; SAPNs formed in 20 mM HEPES pH 7.5, 150 mM NaCl, 5% glycerol, i.e., under close to physiological conditions, were also examined by STEM. As illustrated by Fig. 4, STEM is a powerful method to directly correlate the measured molecular weight of a particle to its shape. The main peak at 2.2 (±0.5) MDa in the mass-distribution clearly corresponds to relatively uniform spherical particles, while the smaller less well-defined peaks at higher molecular weights frequently arise from multiple nanoparticles sticking together (Fig. 4). Accordingly, the mass values of peaks 3 and 4 are also close multiples of 2.23 MDa. SAPNs with a particle mass of 2.23 MDa must be formed by approximately 180 peptide chains, implying that they have a $T = 3$ icosahedron-like structure with a predicted diameter of 25 nm (Fig 1D, bottom). This is in good agreement with the 27 or 28 nm average diameter indicated by TEM and DLS for SAPNS under close to physiological conditions. The second peak in the mass-distribution, 3.8 (±0.5) MDa, implies the presence of particles with approximately 300 peptide chains, which may explain the somewhat elongated structure of some SAPNs. This might be an infrequent unique structure or, as evident for some of the projections, arise from the association of two lower mass SAPNs. It should be noted that the various species documented by STEM were necessarily measured together in the bulk DLS experiment, which will have broadened the single peak obtained and increased the estimated average hydrodynamic size.

The TEM and DLS analyzes of P6c SAPNs formed under different conditions revealed some clear trends and showed that the size distribution of the various species in the samples is influenced by the refolding conditions. The effect of salt concentration was

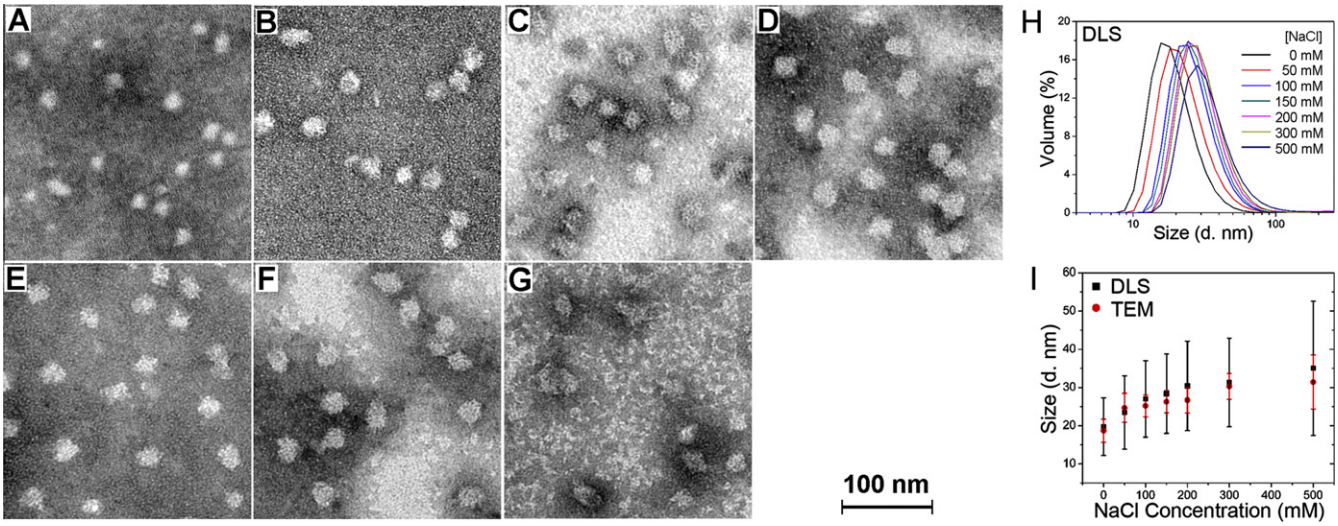

Fig.5. Effect of salt concentration on the SAPNs. TEM images of the SAPNs formed at a peptide concentration of 0.05 mg/ml in 20 mM HEPES pH 7.5 and 5% glycerol at various NaCl concentrations: (A) 0 mM, (B) 50 mM, (C) 100 mM, (D) 150 mM, (E) 200 mM, (F) 300 mM, and (G) 500 mM. All the images have the same scale bar of 100 nm. (H) DLS profiles for volume distribution of hydrodynamic sizes at different salt concentration. (I) The relationship between hydrodynamic size and salt concentration. The black rectangles represent the hydrodynamic diameters of the SAPNs measured by DLS. The red circles represent the diameters of the SAPNs measured by TEM.

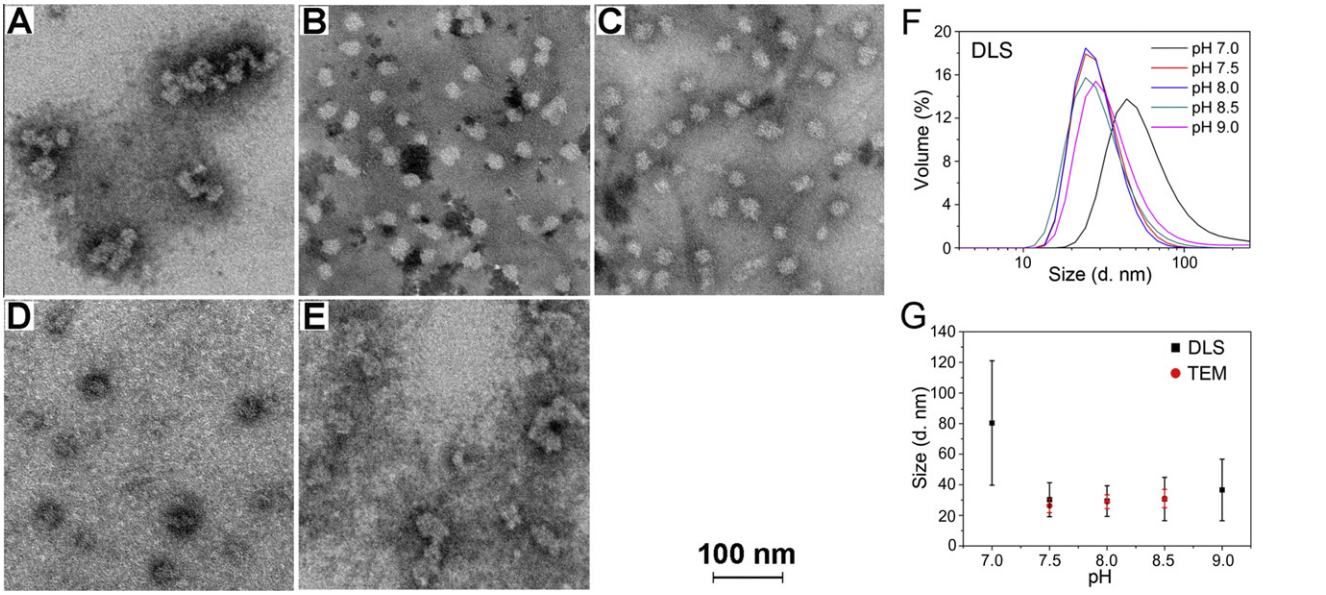

Fig.6. Effect of pH on the SAPNs. TEM images of the SAPNs formed at a peptide concentration of 0.05 mg/ml in the presence of 150 mM NaCl and 5% glycerol in buffers with different pH values: (A) 7.0; (B) 7.5; (C) 8.0; (D) 8.5; and (E) 9.0. The images all have the same scale bar of 100 nm. (F) DLS profiles showing the volume distribution used to calculate the hydrodynamic sizes at different pHs. (G) The relationship between hydrodynamic size and pH. The black rectangles represent the hydrodynamic diameters of the SAPNs measured by dynamic light scattering. The red circles represent the diameters of the SAPNs measured by TEM.

particularly marked indicating that the ionic strength of the buffer solution is important (Fig. 5); larger SAPNs are favored at higher salt concentrations (up to 300 mM NaCl) and above a given ionic strength (between 300 and 500 mM NaCl) particle aggregation becomes more pronounced. The observed size and shape variability of the single nanoparticles probably reflects changes in the geometric packing of the trimeric and pentameric coiled coils of P6c under the different conditions. In the absence of the disulfide bridge of the original construct (compare Fig. 1A and B), the relative angular orientation of these coiled coils will be more sensitive to changes in the interactions within the SAPN (see above). This would explain why the size of the nanoparticles varies and why under certain conditions they appear to be slightly elongated. Both, the stoichiometry and the spacing between coiled-coil neighbors could vary or just one of them. High stoichiometry coupled to decreased coiled-coil spacing would result in the highest possible density of epitopes on SAPN decoration. The SAPNs assembled under close to physiological conditions and in many of the other experiments were larger than expected from the proposed $T = 1$ icosahedral model (Fig. 1D, top). In agreement, as mentioned above STEM indicated three times the expected stoichiometry, 180 peptide chains rather than 60, compatible with a $T = 3$ icosahedal SAPN structure (Fig. 1D, bottom). This will be reflected by the number of epitopes displayed on decoration. Even though the diameter of the particle is larger, the net epitope density at the surface will be higher than the density predicted by the $T = 1$ icosahedral model.

Surprisingly, P6c SAPN assembly was fairly insensitive to changes in buffer system and pH. The only large difference was

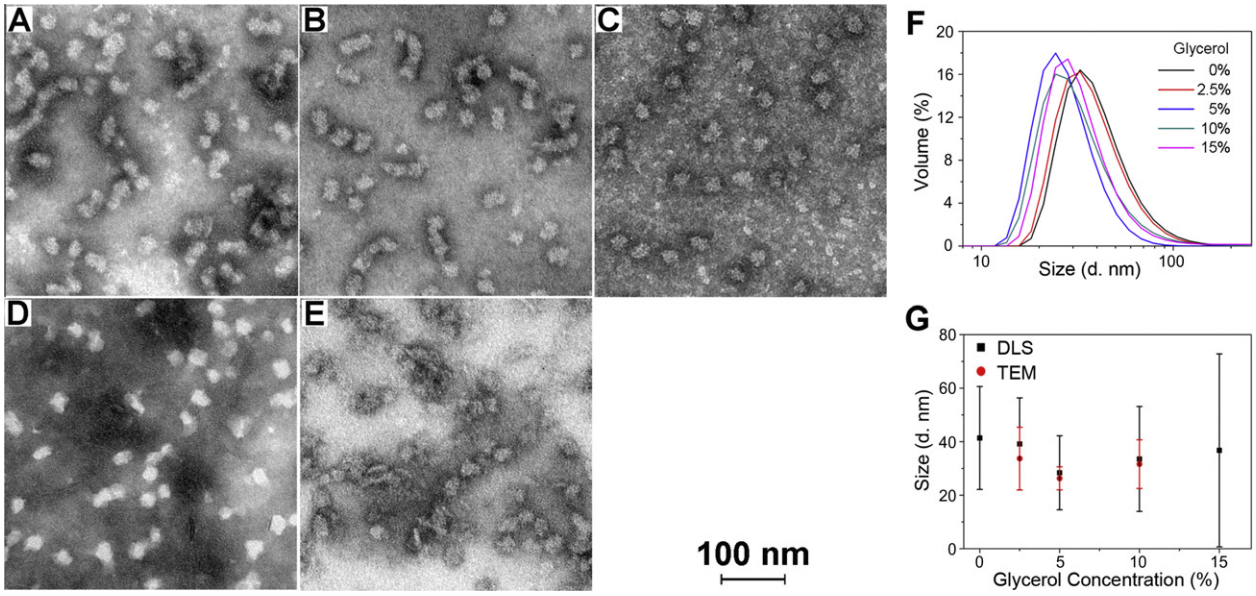

Fig.7. Effect of glycerol concentration on the SAPNs. TEM images of the SAPNs formed at a peptide concentration is 0.05 mg/ml in 20 mM HEPES pH 7.5 and 150 mM NaCl and various glycerol concentrations: (A) 0% v/v glycerol; (B) 2.5% v/v glycerol; (C) 5% v/v glycerol; (D) 10% v/v glycerol; (E) 15% v/v glycerol. The images all have the same scale bar of 100 nm. (F) DLS profiles showing the volume distribution used to calculate the hydrodynamic sizes at different glycerol concentrations. (G) The relationship between hydrodynamic size and glycerol concentration. The black rectangles represent the hydrodynamic diameters of the SAPNs measured by dynamic light scattering. The red circles represent the diameters of the SAPNs measured by TEM.

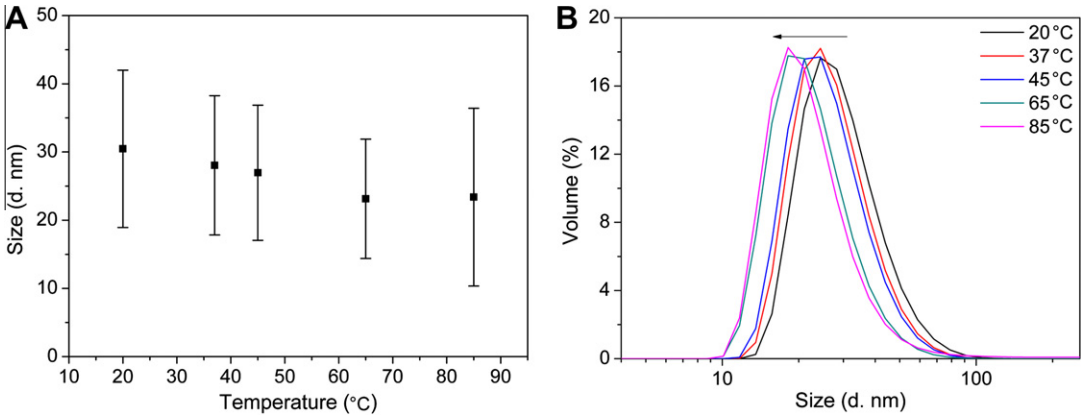

Fig.8. Temperature effects on the SAPNs. The peptide concentration was 0.05 mg/ml. The buffer was 20 mM phosphate pH 7.5, 150 mM NaCl, and 5% glycerol. (A) The relationship between hydrodynamic size and temperature. (B) DLS profiles showing the volume distribution used to calculate the hydrodynamic sizes at different temperature.

when the change was made from pH 7.0 (20 mM BES) to pH 7.5 (20 mM HEPES) (Fig. 6). Glycerol was essential to prevent SAPN aggregation, being most effective at a concentration of 5% v/v. Further, under close to physiological conditions, increasing the temperature had little effect on nanoparticle stability and the SAPNs showed a remarkable thermostability.

As we have observed in recent immunization experiments, the epitope density on SAPNs can significantly affect their immunogenicity (manuscript in preparation). Thus, it is very important to understand the influence refolding conditions have on the dimensions, shape and stoichiometry of SAPNs. As unfavorable conditions can also lead to pronounced aggregation, understanding the influence of the refolding step is also essential to define the best long-term storage conditions for the resulting vaccines. Given the foreseen application of SAPNs, the optimum conditions should also be close to physiological. This is the case for P6c making the SAPNs formed interesting for vaccine development.

Acknowledgments

The authors thank the Institute of Materials Science and the Polymer Program at the University of Connecticut for support of YY. The STEM microscopy was funded by the Maurice E. Müller Foundation of Switzerland and Swiss National Foundation Grant 3100A0-108299 to Andreas Engel; SM and PR thank Andreas Engel and Henning Stahlberg for supporting this STEM project.

References

Aebi, U., ten Heggeler, B., Onorato, L., Kistler, J., Showe, M.K., 1977. New method for localizing proteins in periodic structures: fab fragment labeling combined with image processing of electron micrographs. Proc. Natl. Acad. Sci. USA 74, 5514–5518.

Burkhard, P., Meier, M., Lustig, A., 2000a. Design of a minimal protein oligomerization domain by a structural approach. Protein Sci. 9, 2294–2301.

Burkhard, P., Stetefeld, J., Strelkov, S.V., 2001. Coiled coils: a highly versatile protein folding motif. Trends Cell Biol. 11, 82–88.
Burkhard, P., Ivaninskii, S., Lustig, A., 2002. Improving coiled-coil stability by optimizing ionic interactions. J. Mol. Biol. 318, 901–910.
Burkhard, P., Kammerer, R.A., Steinmetz, M.O., Bourenkov, G.P., Aebi, U., 2000b. The coiled-coil trigger site of the rod domain of cortexillin I unveils a distinct network of interhelical and intrahelical salt bridges. Structure 8, 223–230.
Carlson, J.C.T., Jena, S.S., Flenniken, M., Chou, T.F., Siegel, R.A., et al., 2006. Chemically controlled self-assembly of protein nanorings. J. Am. Chem. Soc. 128, 7630–7638.
Dintzis, H.M., Dintzis, R.Z., Vogelstein, B., 1976. Molecular determinants of immunogenicity: the immunon model of immune response. Proc. Natl. Acad. Sci. USA 73, 3671–3675.
Drexler, K.E., 1981. Molecular engineering: an approach to the development of general capabilities for molecular manipulation. Proc. Natl. Acad. Sci. USA 78, 5275–5278.
Fairman, R., Åkerfeldt, K.S., 2005. Peptides as novel smart materials. Curr. Opin. Struct. Biol. 15, 453–463.
Fehr, T., Skrastina, D., Pumpens, P., Zinkernagel, R.M., 1998. T cell-independent type I antibody response against B cell epitopes expressed repetitively on recombinant virus particles. Proc. Natl. Acad. Sci. USA 95, 9477–9481.
Gazit, E., 2007. Self-assembled peptide nanostructures: the design of molecular building blocks and their technological utilization. Chem. Soc. Rev. 36, 1263–1269.
Holmes, T.C., 2002. Novel peptide-based biomaterial scaffolds for tissue engineering. Trends Biotechnol. 20, 16–21.
Kaba, S.A., Brando, C., Guo, Q., Mittelholzer, C., Raman, S., et al., 2009. A nonadjuvanted polypeptide nanoparticle vaccine confers long-lasting protection against rodent malaria. J. Immunol. 183, 7268–7277.
Kammerer, R.A., Schulthess, T., Landwehr, R., Lustig, A., Engel, J., Aebi, U., Steinmetz, M.O., 1998. An autonomous folding unit mediates the assembly of two-stranded coiled coils. Proc. Natl. Acad. Sci. USA 95, 13419–13424.
Krzyžánek, V., Müller, S.A., Engel, A., Reichelt, R., 2009. MASDET-A fast and user-friendly multiplatform software for mass determination by dark-field electron microscopy. J. Struct. Biol. 165, 78–87.
Malashkevich, V.N., Kammerer, R.A., Efimov, V.P., Schulthess, T., Engel, J., 1996. The crystal structure of a five-stranded coiled coil in COMP: a prototype ion channel? Science 274, 761–765.
Meier, M., Burkhard, P., 2006. Statistical analysis of intrahelical ionic interactions in α-helices and coiled coils. J. Struct. Biol. 155, 116–129.
Meier, M., Stetefeld, J., Burkhard, P., 2010. The many types of interhelical ionic interactions in coiled coils – an overview. J. Struct. Biol. 170, 192–201.
Meier, M., Lustig, A., Aebi, U., Burkhard, P., 2002. Removing an interhelical salt bridge abolishes coiled-coil formation in a de novo designed peptide. J. Struct. Biol. 137, 65–72.
Meng, F.G., Park, Y.D., Zhou, H.M., 2001. Role of proline, glycerol, and heparin as protein folding aids during refolding of rabbit muscle creatine kinase. Int. J. Biochem. Cell Biol. 33, 701–709.
Müller, S.A., Goldie, K.N., Bürki, R., Häring, R., Engel, A., 1992. Factors influencing the precision of quantitative scanning transmission electron microscopy. Ultramicroscopy 46, 317–334.
O'Shea, E.K., Klemm, J.D., Kim, P.S., Alber, T., 1991. X-ray structure of the GCN4 leucine zipper, a two-stranded, parallel coiled coil. Science 254, 539–544.
Padilla, J.E., Colovos, C., Yeates, T.O., 2001. Nanohedra: using symmetry to design self assembling protein cages, layers, crystals, and filaments. Proc. Natl. Acad. Sci. USA 98, 2217–2221.
Petka, W.A., Harden, J.L., McGrath, K.P., Wirtz, D., Tirrell, D.A., 1998. Reversible hydrogels from self-assembling artificial proteins. Science 281, 389–392.
Pimentel, T.A.P.F., Yan, Z., Jeffers, S.A., Holmes, K.V., Hodges, R.S., et al., 2009. Peptide nanoparticles as novel immunogens: design and analysis of a prototypic severe acute respiratory syndrome vaccine. Chem. Biol. Drug Design 73, 53–61.
Rajagopal, K., Schneider, J.P., 2004. Self-assembling peptides and proteins for nanotechnological applications. Curr. Opin. Struct. Biol. 14, 480–486.
Raman, S., Machaidze, G., Lustig, A., Aebi, U., Burkhard, P., 2006. Structure-based design of peptides that self-assemble into regular polyhedral nanoparticles. Nanomedicine 2, 95–102.
Raman, S., Machaidze, G., Lustig, A., Olivieri, V., Aebi, U., et al., 2009. Design of peptide nanoparticles using simple protein oligomerization domains. Open Nanomed. J. 2, 15–26.
Rapaport, H., Kjaer, K., Jensen, T.R., Leiserowitz, L., Tirrell, D.A., 2000. Two-dimensional order in β-sheet peptide monolayers. J. Am. Chem. Soc. 122, 12523–12529.
Rasband, W.S. ImageJ, US National Institutes of Health, Bethesda, Maryland, USA, <http://imagej.nih.gov/ij/>, vol. 1997.
Scanlon, S., Aggeli, A., 2008. Self-assembling peptide nanotubes. Nano Today 3, 22–30.
Schein, C.H., 1990. Solubility as a function of protein structure and solvent components. BioTechnology 8, 308–317.
Schroeder, U., Graff, A., Buchmeier, S., Rigler, P., Silvan, U., et al., 2009. Peptide nanoparticles serve as a powerful platform for the immunogenic display of poorly antigenic actin determinants. J. Mol. Biol. 386, 1368–1381.
Stetefeld, J., Jenny, M., Schulthess, T., Landwehr, R., Engel, R.A., et al., 2000. Crystal structure of a naturally occurring parallel right-handed coiled coil tetramer. Nat. Struct. Biology 7, 772–776.
Subramani, K., Khraisat, A., George, A., 2008. Self-assembly of proteins and peptides and their applications in bionanotechnology. Curr. Nanosci. 4, 201–207.
Tao, Y., Strelkov, S.V., Mesyanzhinov, V.V., Rossmann, M.G., 1997. Structure of bacteriophage T4 fibritin: a segmented coiled coil and the role of the C-terminal domain. Structure 5, 789–798.
Toksöz, S., Guler, M.O., 2009. Self-assembled peptidic nanostructures. Nano Today 4, 458–469.
Tsai, C.J., Zheng, J., Zanuy, D., Haspel, N., Wolfson, H., et al., 2007. Principles of nanostructure design with protein building blocks. Proteins 68, 1–12.
Whitesides, G.M., Boncheva, M., 2002. Beyond molecules: self-assembly of mesoscopic and macroscopic components. Proc. Natl. Acad. Sci. USA 99, 4769–4774.
Whitesides, G.M., Grzybowski, B., 2002. Self-assembly at all scales. Science 295, 2418–2421.
Yang, Y.L., Khoe, U., Wang, X.M., Horii, A., Yokoi, H., et al., 2009. Designer self-assembling peptide nanomaterials. Nano Today 4, 193–210.
Zandi, R., Reguera, D., Bruinsma, R.F., Gelbart, W.M., Rudnick, J., 2004. Origin of icosahedral symmetry in viruses. Proc. Natl. Acad. Sci. USA 101, 15556–15560.
Zanuy, D., Nussinov, R., Alemán, C., 2006. From peptide-based material science to protein fibrils: discipline convergence in nanobiology. Physical Biol. 3.
Zhang, S., Gelain, F., Zhao, X., 2005. Designer self-assembling peptide nanofiber scaffolds for 3D tissue cell cultures. Semin. Cancer Biol. 15, 413–420.
Zhang, S.G., 2002. Emerging biological materials through molecular self-assembly. Biotechnol. Adv. 20, 321–339.
Zhang, S.G., 2003. Fabrication of novel biomaterials through molecular self-assembly. Nat. Biotechnol. 21, 1171–1178.
Zhang, S.G., Marini, D.M., Hwang, W., Santoso, S., 2002. Design of nanostructured biological materials through self-assembly of peptides and proteins. Curr. Opin. Chem. Biol. 6, 865–871.